Remote Sensing of Environment 211 (2018) 204–217

Contents lists available at ScienceDirect

Remote Sensing of Environment

journal homepage: www.elsevier.com/locate/rse

The SMAP mission combined active-passive soil moisture product at 9 km and 3 km spatial resolutions

Narendra N. Das[a,*], Dara Entekhabi[b], R. Scott Dunbar[a], Andreas Colliander[a], Fan Chen[c], Wade Crow[d], Thomas J. Jackson[d], Aaron Berg[e], David D. Bosch[f], Todd Caldwell[g], Michael H. Cosh[h], Chandra H. Collins[i], Ernesto Lopez-Baeza[j], Mahta Moghaddam[k], Tracy Rowlandson[e], Patrick J. Starks[l], Marc Thibeault[m], Jeffrey P. Walker[n], Xiaoling Wu[n], Peggy E. O'Neill[o], Simon Yueh[a], Eni G. Njoku[a]

[a] *Jet Propulsion Laboratory, California Institute of Technology, Pasadena, CA 91109, USA*
[b] *Massachusetts Institute of Technology, Cambridge, MA 02139, USA*
[c] *Science System and Application, Inc, United State Department of Agriculture, Beltsville, Maryland, USA*
[d] *United State Department of Agriculture, Beltsville, Maryland, USA*
[e] *University of Guelph, Canada*
[f] *USDA ARS Southeast Watershed Research, Tucson, AZ, USA*
[g] *University of Texas at Austin, Texas, USA*
[h] *USDA ARS Hydrology and Remote Sensing Laboratory, Beltsville, MD, USA*
[i] *USDA ARS Southwest Watershed Research, Tucson, AZ, USA*
[j] *University of Valencia, Spain*
[k] *University of Southern California, California, USA*
[l] *USDA ARS Grazinglands Research Laboratory, El Reno, OK, USA*
[m] *Comisión Nacional de Actividades Espaciales (CONAE), Argentina*
[n] *Monash University, Australia*
[o] *Goddard Space Flight Center (GSFC), NASA, 8800 Greenbelt, MD 20771, USA*

A R T I C L E I N F O

Keywords:
SMAP
Microwave remote sensing
Soil moisture
Active and passive

A B S T R A C T

The NASA Soil Moisture Active Passive (SMAP) mission was launched on January 31st, 2015. The spacecraft was to provide high-resolution (3 km and 9 km) global soil moisture estimates at regular intervals by combining for the first time L-band radiometer and radar observations. On July 7th, 2015, a component of the SMAP radar failed and the radar ceased operation. However, before this occurred the mission was able to collect and process ~2.5 months of the SMAP high-resolution active-passive soil moisture data (L2SMAP) that coincided with the Northern Hemisphere's vegetation green-up and crop growth season. In this study, we evaluate the SMAP high-resolution soil moisture product derived from several alternative algorithms against *in situ* data from core calibration and validation sites (CVS), and sparse networks. The baseline algorithm had the best comparison statistics against the CVS and sparse networks. The overall unbiased root-mean-square-difference is close to the 0.04 m^3/m^3 the SMAP mission requirement. A 3 km spatial resolution soil moisture product was also examined. This product had an unbiased root-mean-square-difference of ~0.053 m^3/m^3. The SMAP L2SMAP product for ~2.5 months is now validated for use in geophysical applications and research and available to the public through the NASA Distributed Active Archive Center (DAAC) at the National Snow and Ice Data Center (NSIDC). The L2SMAP product is packaged with the geo-coordinates, acquisition times, and all requisite ancillary information. Although limited in duration, SMAP has clearly demonstrated the potential of using a combined L-band radar-radiometer for proving high spatial resolution and accurate global soil moisture.

* Corresponding author.
E-mail addresses: Nndas@jpl.nasa.gov (N.N. Das), Darae@mit.edu (D. Entekhabi), Roy.S.Dunbar@jpl.nasa.gov (R.S. Dunbar), Andreas.Colliander@jpl.nasa.gov (A. Colliander), Fan.Chen@ars.usda.gov (F. Chen), Wade.Crow@ars.usda.gov (W. Crow), Tom.jackson@ars.usda.gov (T.J. Jackson), aberg@uoguelph.ca (A. Berg), David.Bosch@ars.usda.gov (D.D. Bosch), todd.caldwell@beg.utexas.edu (T. Caldwell), Michael.Cosh@ars.usda.gov (M.H. Cosh), chandra.holifield@ars.usda.gov (C.H. Collins), Ernesto.Lopez@uv.es (E. Lopez-Baeza), mahta@usc.edu (M. Moghaddam), trowland@uoguelph.ca (T. Rowlandson), Patrick.Starks@ars.usda.gov (P.J. Starks), mthibeault@conae.gov.ar (M. Thibeault), jeff.walker@monash.edu.au (J.P. Walker), xiaoling.wu@monash.edu.au (X. Wu), Peggy.E.O'Neill@nasa.gov (P.E. O'Neill), Simon.Yueh@jpl.nasa.gov (S. Yueh).

https://doi.org/10.1016/j.rse.2018.04.011
Received 20 October 2016; Received in revised form 30 March 2018; Accepted 5 April 2018

1. Introduction

NASA's Soil Moisture Active Passive (SMAP) mission was launched on January 31st, 2015. The objective of the mission is global mapping of high-resolution surface soil moisture and landscape freeze/thaw state (Entekhabi et al., 2010). SMAP utilizes an L-band radar and radiometer sharing a rotating 6-meter mesh reflector antenna. The SMAP spacecraft is in a 685-km Sun-synchronous near-polar orbit and views the surface at a constant 40-degree incidence angle with a 1000-km swath width. The basic premise of the mission was that merging of the high-resolution active (radar) and coarse-resolution but high-sensitivity passive (radiometer) L-band observations would enable an unprecedented combination of accuracy, resolution, coverage, and revisit-time for soil moisture and freeze/thaw state retrievals (Entekhabi et al., 2010; Das et al., 2014). However, on July 7th, 2015, the SMAP radar ceased operations due to a component failure. As a result, the observatory was only able to provide ~2.5 months (from the end of In-Orbit-Check April 13th, 2015 to July 7th, 2015) of the SMAP active-passive product (L2SMAP) (the radiometer continues to be fully operational). The product is based on downscaling of gridded 36 km SMAP brightness temperature (T_{B_p}) data to a higher spatial resolution (9 km) using SMAP radar backscatter observations and the subsequent inversion of the resulting high-resolution T_{B_p} fields into soil moisture retrievals. Another higher resolution at 3 km global surface soil moisture data set is also produced for assessment and potential implementation.

Prior to this investigation, the active-passive algorithm (presented in subsequent section) had only been implemented with simulated data and limited aircraft-based observations. The work presented here shows the operational capability of the SMAP active-passive algorithm and provides a calibration/validation of the products using various core sites. Although the duration of the L2SMAP is only ~2.5 months (due to the malfunction of the SMAP radar), within this period, it provided a demonstration that the active-passive algorithm could work under all hydroclimatic domains with moderate and heterogeneous vegetation cover. The product also provided the first satellite demonstration of the effectiveness of using the combination of L-band radar and radiometer observations as an effective approach to high spatial resolution and accurate soil moisture retrieval. Hence, this product supports the development of this approach in current and future missions.

2. Active-passive algorithm review

In the past, numerous studies (Kim and Barros, 2002; Kim and Barros, 2003; Chauhan et al., 2003; and Reichle et al., 2001) have attempted to obtain high-resolution soil moisture by downscaling coarse resolution (~50 km) soil moisture products from satellite-based microwave radiometers. These studies used high-resolution remote sensing observations and fine-scale ancillary geophysical information such as topography, vegetation, soil type, and precipitation that exert physical control over the evolution of soil moisture. For example, high-resolution thermal infrared data from MODIS and soil parameters were utilized in a deterministic approach to disaggregate the SMOS ~40 km soil moisture product to a ~1 km soil moisture estimate (Molero et al., 2016; Merlin et al., 2008). A common factor in these approaches is the use of static and dynamic geophysical data in the downscaling/disaggregation approach. The geophysical observations come from different sources with some inherent errors, as well as temporal registration mismatch that can affect the accuracy of the downscaled soil moisture estimates. For example, the MODIS thermal infrared data is measured at ~10:00 AM local time and are not co-registered (in the SMAP mission the radar and radiometer observations are acquired at the same time *i.e.*, ~6:00 AM for descending orbits) along with the satellite-based radiometer observations (SMAP and SMOS). This mismatch of observation times can change the surface soil moisture spatial pattern. The MODIS thermal infrared penetration depth is also very shallow (skin deep) as compared to the penetration depth of ~5 cm or more for the satellite-based L-band microwave radiometer observations. SMAP mitigates these sources of errors by the use of co-registered and concurrent L-band radiometer and the L-band radar observations.

Only a few studies have been conducted that attempted to merge high-resolution radar and coarse resolution radiometer measurements in order to obtain an intermediate resolution product. Change detection techniques have demonstrated a potential to monitor temporal evolution of soil moisture by taking advantage of the approximately linear dependence of radar backscatter and brightness temperature change on soil moisture change. The feasibility of using the change detection approach was demonstrated with the Passive and Active L-band System airborne sensor (PALS) radar and radiometer data obtained during the SGP99 campaign (Narayan et al., 2006). A similar approach was also used to downscale PALS radiometer data with AIRSAR (radr) data from the SMEX02 campaign. The limitation of this technique is that it only provides the soil moisture relative change and not the absolute value of soil moisture. As a consequence, the errors can accumulate because the cumulative errors propagate over a time period.

A different approach is presented in Zhan et al. (2006) where a Bayesian method is used to downscale radiometer observations using radar measurements. Kim and van Zyl (2009) developed a time-series algorithm based on a linear model of backscatter and soil moisture. In order to estimate soil moisture at intermediate resolution (9 km), they determine the two unknowns of the linear model for each pixel within the coarser radiometer pixel. Piles et al. (2009) presented another change detection scheme compatible with SMAP that uses the approximately linear dependence of change in radar backscatter on soil moisture change at radiometer resolution, the temporal change in backscatter at the radar resolution and the previous day's soil moisture data to estimate soil moisture at ~9 km resolution. This is similar to Narayan et al. (2006) but also suffers from the accumulation of errors over time. A spatial variability technique developed by Das et al. (2012) to blend SMAP radar measurement and radiometer-based soil moisture data also takes advantage of the approximately linear dependence of backscatter change to soil moisture change at the radiometer resolution, which constraints the relative backscatter difference within the coarse radiometer footprint, to estimate soil moisture at ~9 km resolution. Unlike Zhan et al. (2006) and Piles et al. (2009), the spatial variability technique used in Das et al. (2012) does not require the previous satellite overpass observations to estimate the current soil moisture value. The SMAP active-passive algorithm (Das et al., 2014) draws from all the above algorithms and techniques (Molero et al., 2016; Merlin et al., 2008; Zhan et al., 2006; Narayan et al., 2006; Kim and van Zyl, 2009; Piles et al., 2009; Das et al., 2012). In particular, it downscales the coarse-scale radiometer-based gridded brightness temperature using the fine resolution radar backscatter, and then near-surface soil moisture is retrieved from the downscaled brightness temperature (Fig. 1).

The SMAP active-passive algorithm (Das et al., 2014) has two parameters ($\boldsymbol{\beta}$ (K/dB) and dimensionless Γ), as shown in Eq. (1).

$$T_{B_p}(M_j) = T_{B_p}(C) + \boldsymbol{\beta}(C)\cdot\{[\sigma_{pp}(M_j) - \sigma_{pp}(C)] + \boldsymbol{\Gamma}\cdot[\sigma_{pq}(C) - \sigma_{pq}(M_j)]\} \tag{1}$$

where $T_{B_p}(M_j)$ is the disaggregated brightness temperature (V-pol or H-pol) at 9 km or 3 km, $T_{B_p}(C)$ is the gridded radiometer brightness temperature (V-pol or H-pol) at 36 km, $\sigma_{pp}(M_j)$ and $\sigma_{pq}(M_j)$ are the co-pol and cross-pol radar backscatters at the corresponding resolution (9 km or 3 km), and $\sigma_{pp}(C_j)$ and $\sigma_{pq}(C_j)$ are the co-pol and cross-pol radar backscatters aggregated to 36 km. The notation M_j represents one of the indexed (j) medium resolution grid cells within the coarse resolution '*C*'. A comprehensive description and physical basis of Eq. (1) is presented in Entekhabi et al., (2010) and Das et al. (2014). However, for the sake of brevity, clarity and completeness Eq. (1) can be summarized as follow:

$T_{B_p}(M_j) =$ *Disaggregated brightness temperature at* 9 *km or* 3 *km*.

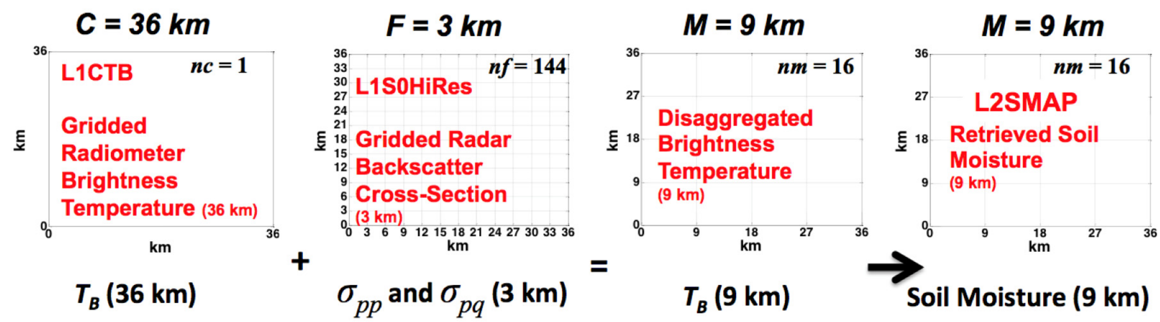

Fig. 1. Schematic representation of the SMAP baseline active-passive algorithm. L1CTB is the gridded T_B product and L1S0HiRes is the gridded σ_{pp} and σ_{pq} product. The value of $nc = 1$, $nf = 144$ and $nm = 16$ are the number of grid cells of $T_B(C)$, $\sigma_{pp}(F)$ and $\sigma_{pq}(F)$, and downscaled $T_B(M)$, respectively, involved in the SMAP active-passive algorithm. Where '*C*' stands for coarse spatial resolution (36 km), '*M*' stands for medium spatial resolution (9 km), and '*F*' stands for fine spatial resolution (3 km).

$T_{B_p}(C) +$ *Parent scale (C) radiometer brightness temperature.*

$\boldsymbol{\beta}(C)\cdot[\sigma_{pp}(M_j) - \sigma_{pp}(C)] +$ *Scale (C) parameter* $\boldsymbol{\beta}$ *times smaller scale*

– M variations

in σ_{pp} *mostly due to soil moisture variability.*

$\boldsymbol{\Gamma}\cdot[\sigma_{pq}(C) - \sigma_{pq}(M_j)]\}$ *Scale (M) heterogeneity parameter* $\boldsymbol{\Gamma}$

times smaller scale (M)

variation in σ_{pq}

mostly due to vegetation and roughness.

For a more comprehensive description of Eq. (1) see Entekhabi et al. (2010) and Das et al. (2014). The proposed SMAP active-passive algorithm Eq. (1) is preferred over alternative algorithms (Zhan et al., 2006; Kim and van Zyl, 2009; Piles et al., 2009; Das et al., 2012) due to the following attributes: i) its inputs (observations) come directly from the SMAP instruments; ii) the algorithm uses a physical basis to derive the Eq. (1); and iii) parameters $\boldsymbol{\beta}(C)$ and Γ are also physically-based and can be analytically derived (as shown in Entekhabi et al. (2010), Das et al. (2014) and Jagdhuber et al. (2015) from radiative transfer physics. The algorithm (Eq. (1)) has also been successfully applied to field campaign data from SMEX02 (Das et al., 2014) and SMAPVEX12 (Leroux et al., 2016; Leroux et al., 2017). Moreover, the disaggregated $T_{B_p}(M_j)$ is used to retrieve soil moisture using the Tau-Omega model, which makes it consistent with the SMAP radiometer-only soil moisture (L2SMP) product.

The disaggregated brightness temperature $T_B(M_j)$ is an intermediate product of the active-passive algorithm. The SMAP active-passive algorithm conserves the energy in the brightness temperature space (T_{B_p}), *i.e.*, the aggregated average of the $T_{B_p}(M_j)$ is equal to $T_{B_p}(C)$, alternative representation is $T_{B_p}(C) \approx \frac{1}{nm}\sum_{j=1}^{nm} T_{B_p}(M_j)$, where nm is the number of high resolution grid cells within a coarse resolution 36 km grid cell (*e.g.*, nm = 16 at 9 km resolution).

Another feature of the SMAP active-passive algorithm is that it is possible to perform disaggregation three different ways. Fig. 2 illustrates these (Option 1, Option 2, and Option 3) ways of implementing Eq. (1). All three options produce 9 km soil moisture; however, they differ based on the scales at which downscaled the TBs are obtained before retrieving soil moisture. The SMAP active-passive baseline algorithm is Option 1. All the options are included in the L2SMAP product file. The advantages of Option 2 and Option 3 are: i) the downscaling of SMAP T_B from 36 km to 3 km resolution; and ii) the retrieval of soil moisture at 3 km resolution. All three options are also implemented for $T_{B_V}(C)$ and $T_{B_H}(C)$ leading to a total of six options at 9 km for soil moisture retrieval. Besides these six options, the L2SMAP product also contains two soil moisture retrievals at 3 km obtained from disaggregated $T_{B_V}(F)$ and $T_{B_H}(F)$. However, the disaggregated $T_{B_V}(M)$ at 9 km obtained by disaggregating $T_{B_V}(C)$ using Option 1 is the SMAP active-passive baseline algorithm. The following sections discuss about the selection of this option as the baseline algorithm.

3. SMAP active-passive (L2SMAP) product

At National Snow and Ice Data Center (NSIDC) Distributed Active Archive Center (DAAC), the L2SMAP data is only available for ~2.5 months (April 13th, 2016 through July 7th, 2016) period because the SMAP radar is inoperable beyond July 7th, 2015. Following this date, the SMAP active-passive algorithm was discontinued due to a lack of SMAP radar data (L1S0HiRes). Therefore, this section elaborates on the results of the L2SMAP product for the ~2.5 months duration only.

3.1. Stability of SMAP active-passive algorithm parameters

The performance of the brightness temperature disaggregation that results in the 9 km or 3 km soil moisture retrievals is heavily dependent on obtaining robust estimates of the parameters $\boldsymbol{\beta}$ and Γ in Eq. (1). Regressions of the time-series (based on multiple overpasses) for $T_{B_p}(C)$ and $\sigma_{pp}(C)$ are used to statistically estimate $\boldsymbol{\beta}$. The statistically-estimated slope parameters are specific for a given location, and reflect local roughness and vegetation cover conditions under the assumption that they are fairly stable during the time period of $\boldsymbol{\beta}$ estimation. The parameter Γ is also determined statistically for any particular overpass, using the radar backscatters σ_{pp} and σ_{pq} at the finest available resolution (in this case at 3 km) that are encompassed within the 36 km $T_{B_p}(C)$ grid cell.

Fig. 3 illustrates the distribution of the $\boldsymbol{\beta}$ parameter in the emissivity/dB (–/dB) term. Before its application in Eq. (1), the $\boldsymbol{\beta}$ parameter is multiplied with land surface temperature to convert to the K/dB term. The $\boldsymbol{\beta}$ parameter values obtained were found to be consistent with the values that are derived from the analysis of the soil moisture field experiments (SGP99, SMEX02, CLASIC, and SMAPVEX08), and 3 years of Aquarius data.

Values (magnitude) of the $\boldsymbol{\beta}$ parameter over arid regions like the Sahara Desert are lower than expected. The reason for this bias is the absence of a dynamic range of conditions over arid regions within the limited duration (~2.5 months) of available data. Fig. 4 shows the correlation map of $T_{B_V}(C)$ and $\sigma_{vv}(C)$ for the ~2.5 month period. The map (Fig. 4) also represents the statistical robustness of the estimated $\boldsymbol{\beta}$ parameter. High correlations are observed globally over most land surfaces except for the arid and heavily forested regions. This inferior quality of $\boldsymbol{\beta}$ parameter estimates over the arid regions and the heavily forested regions is due to the lack of dynamic range in $T_{B_p}(C)$ and $\sigma_{pp}(C)$. Moreover, in the heavily forested regions, the lack of dynamic range in $T_{B_p}(C)$ and $\sigma_{pp}(C)$ can be attributed to the high volume scattering and a

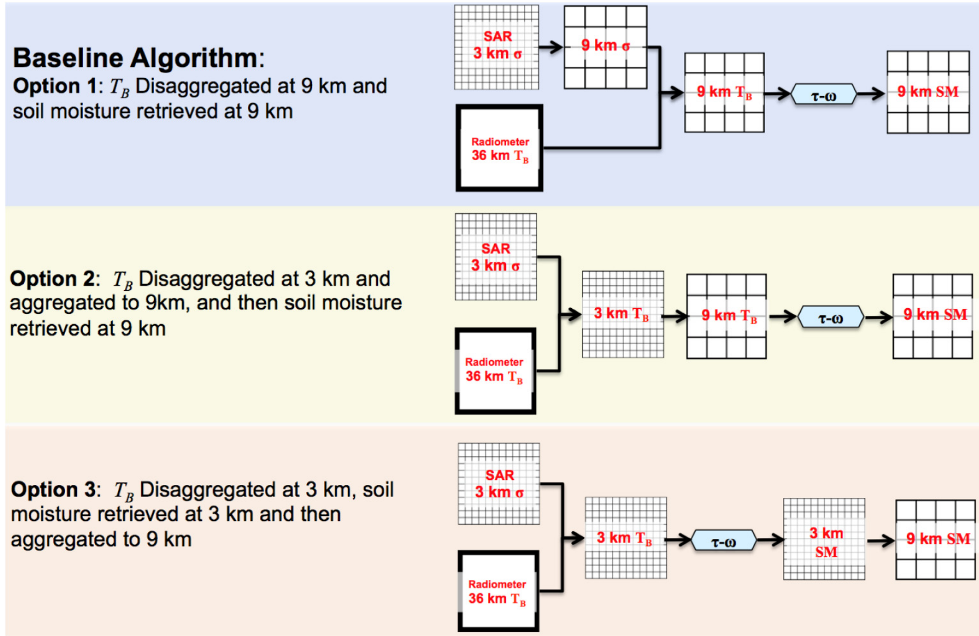

Fig. 2. Different implementations of the SMAP active-passive algorithm in the SMAP Science Production Software (SPS).

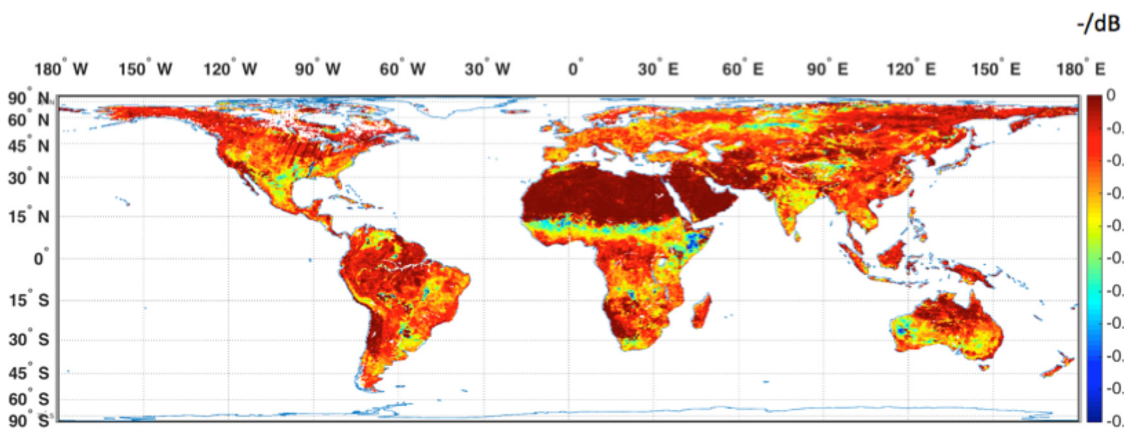

Fig. 3. $\boldsymbol{\beta}$ parameter computed using all the available SMAP radar (vv-pol) and radiometer (V-pol) data from April 15, 2015 to July 7th, 2015. The **β** parameter is actually determined in emissivity/dB terms.

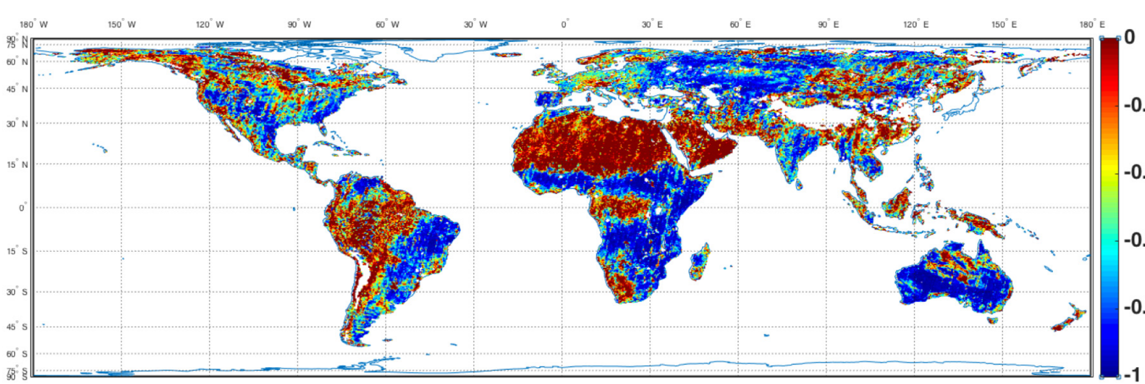

Fig. 4. Correlation map of $T_{B_v}(C)$ and $\sigma_{vv}(C)$ computed using all the available SMAP radar (vv-pol) and radiometer (V-pol) data from April 15, 2015 to July 7th, 2015.

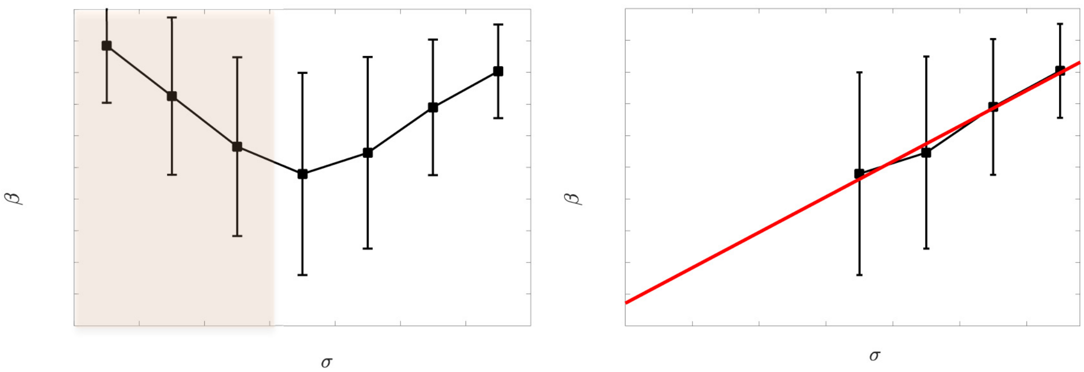

Fig. 5. Trend in $\boldsymbol{\beta}$ parameter with respect to the SMAP radar cross-pol σ_{hv} data. (a) The full trend of $\boldsymbol{\beta}$ that includes parameters over barren deserts shown as shaded region. (b) The curtailed version that is used to derive a regression model (red line) for $\boldsymbol{\beta}$ parameters used in the SMAP active-passive algorithm for the grid cells where derived $\boldsymbol{\beta}$ is inferior or the correlation coefficient (Fig. 4) is below 0.5. (For interpretation of the references to colour in this figure legend, the reader is referred to the web version of this article.)

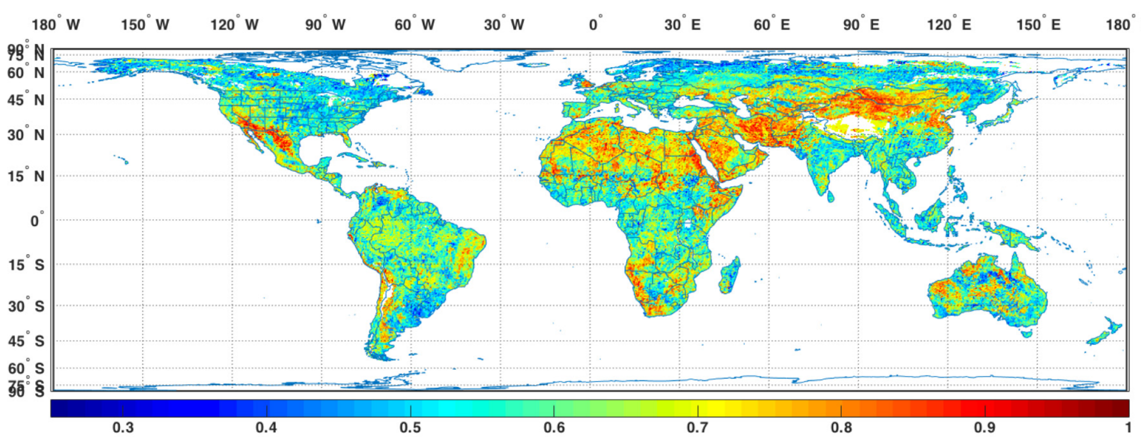

Fig. 6. Map of Γ parameter at global extent averaged for 04-28-2015 to 05-28-2015.

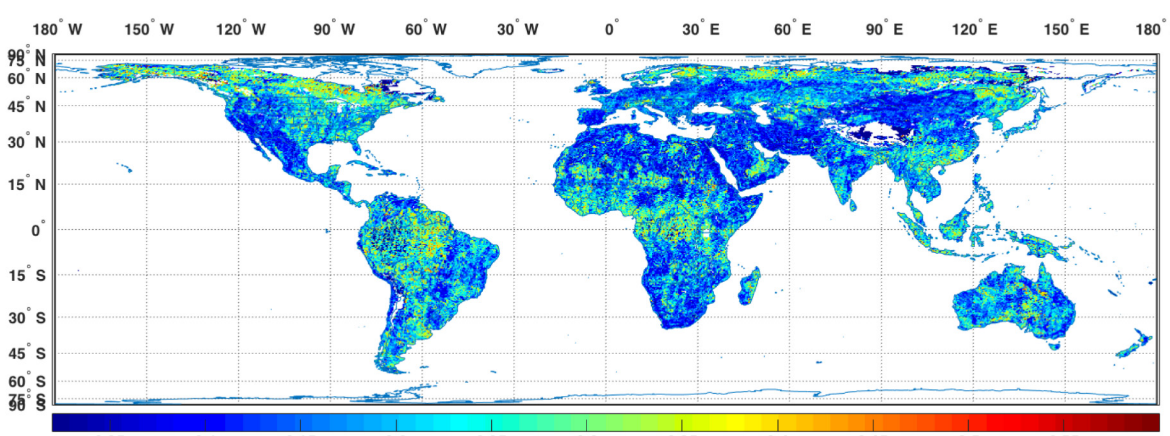

Fig. 7. Coefficient of variation of Γ parameter computed for 04-28-2015 to 05-28-2015.

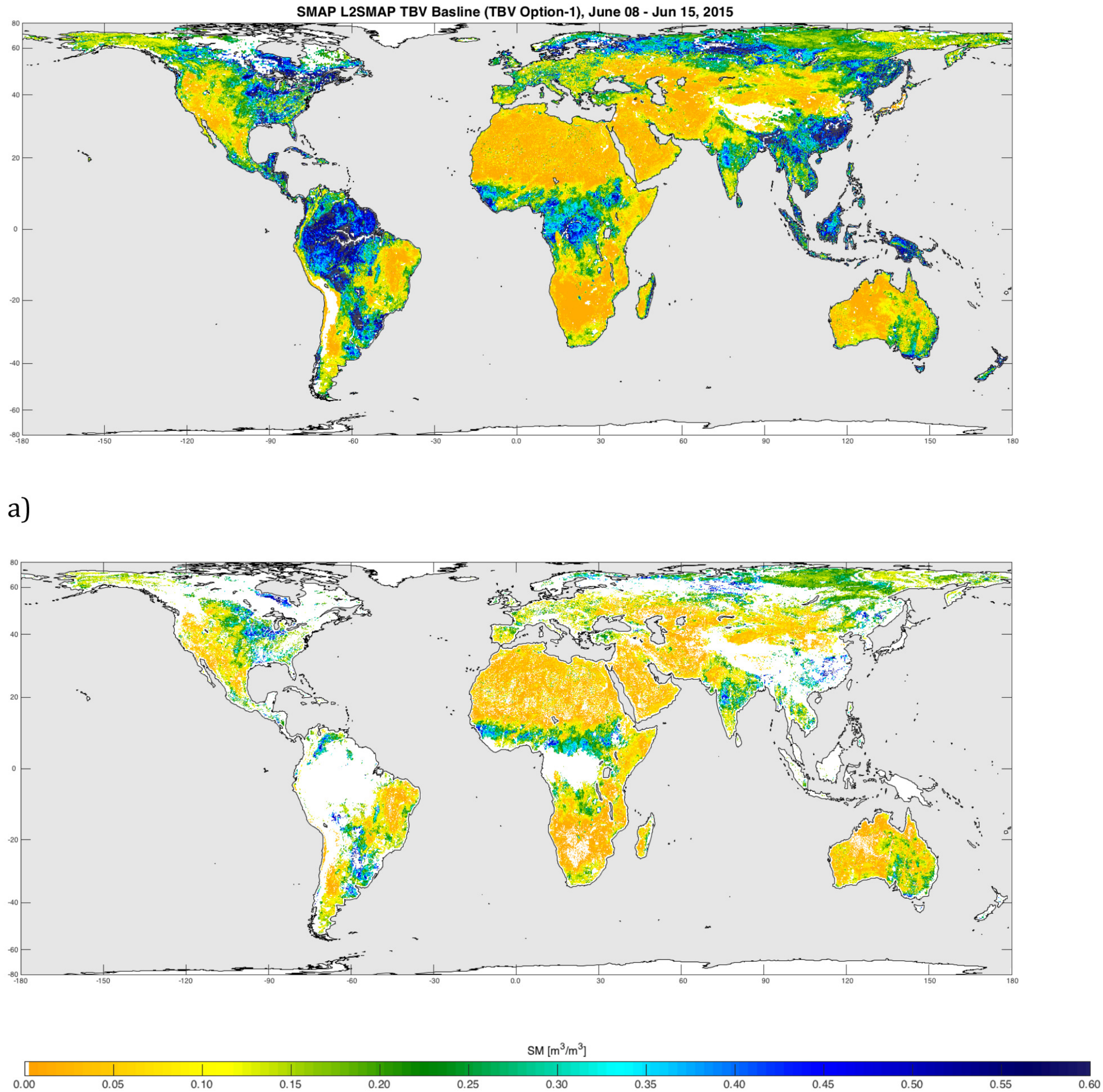

Fig. 8. SMAP L2SMAP (TBV) Option-1 global images with flags (a) and with cleared flags (b) for soil moisture products.

lack of sensitivity to the underlying soil layer. Fig. 5 shows the trend in the $\boldsymbol{\beta}$ parameter against the σ_{pq} SMAP radar backscatter is associated with the level of vegetation. An almost linear trend (shown as the red line in Fig. 5b) is observed in the $\boldsymbol{\beta}$ parameter with respect to SMAP radar $\sigma_{pq}$for the regions where the correlation is high. The nonlinearity in the $\boldsymbol{\beta}$ parameter trend for σ_{pq} radar data less than -25 [dB] (Fig. 5a) is due to inadequate (less than ~2.5 months) time series data that leads to inferior estimation. Given the dynamic range of $T_{B_p}(C)$ and $\sigma_{pp}(C)$ over arid regions, the trend should follow the red line. Therefore, in the L2SMAP algorithm implementation, the model that follows the red line as shown in Fig. 5 is used where the $\boldsymbol{\beta}$ parameter estimation is higher correlation than 0.5.

The algorithm parameter Γ exhibits more temporal stability as compared to the $\boldsymbol{\beta}$ parameter. Fig. 6 shows the global distribution of the Γ parameter. The range of values of Γ parameter corresponds with the parameters derived from the soil moisture field campaigns (SGP99, SMEX02, CLASIC, and SMAPVEX08) data. To evaluate the stability of the Γ parameter, the coefficient of variation was computed for one-month period as shown in Fig. 7. The coefficient of variation is very low for the most regions of the world suggesting stability in derived Γ parameter.

3.2. Patterns and features in the SMAP L2SMAP product

The L2SMAP product was analyzed at 9 km and 3 km using the various options (as discussed in Section 3.1). The results shown henceforth are composited (averaged) for 7 days to provide a complete global extent of soil moisture evolution over different biomes and landcovers. Assessment of global soil moisture from the SMAP active-passive retrievals shows consistency in the soil moisture range

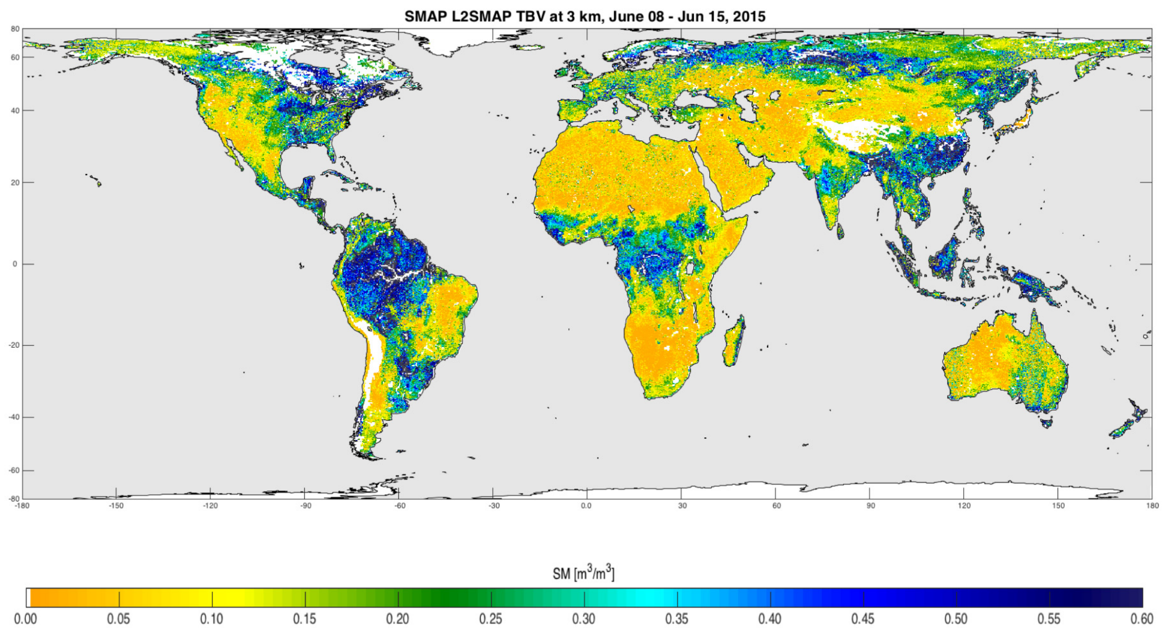

Fig. 9. SMAP L2SMAP (TBV) 3 km soil moisture global composite.

($0.02\,m^3/m^3$ to $0.5\,m^3/m^3$) and probable values. For example, the regions that are very dry (*i.e.*, the Sahara desert) and wet (*i.e.*, the Amazon Basin) reflect the nature of the oil moisture distribution and expected variability as influenced by geophysical factors (soil types, vegetation, weather, and terrain) and landcovers. However, further evaluation of the soil moisture estimates was conducted over a limited set of core validation sites (CVS) to evaluate the accuracy and performance of the SMAP active-passive retrievals. Fig. 8a illustrates the soil moisture retrievals using the downscaled T_{B_v} at 9 km obtained from the SMAP baseline (Option-1) active-passive algorithm. Fig. 8b is the same as Fig. 8a, except only showing data with valid quality flags. The regions with valid (cleared of all quality flags) soil moisture data as shown in Fig. 8b are those that meet the SMAP Level-1 requirements (SMAP mission Level-1 requirement: the baseline science mission shall provide estimates of soil moisture in the top 5 cm of soil with an error of no greater than $0.04\,m^3/m^3$ volumetric (one sigma) at 10 km spatial resolution and 3-day average intervals over the global land area excluding regions of snow and ice, frozen ground, mountainous topography, open water, urban areas, and vegetation with water content greater than $5\,kg/m^2$). Similarly, Fig. 9 shows the 3 km soil moisture retrievals from the SMAP active-passive algorithm generated using the Option-3 implementation approach discussed in the previous section. To illustrate the difference between the various resolutions of the SMAP products and the skill of the SMAP active-passive algorithm to capture spatial details and heterogeneity with the radiometer coarse observation and soil moisture retrievals, a comparison is presented in Fig. 10. The variability within the radiometer coarse grid cell is mostly due to soil moisture, vegetation and soil roughness, and is captured by high-resolution SMAP radar backscatter values of σ_{pp} and σ_{pq} at the finest available resolution (in this case at 3 km). Fig. 10 clearly shows the capability of the baseline algorithm (Eq. (1)) to get high-resolution brightness temperature data and subsequent soil moisture retrievals using the fine scale information obtained from the high-resolution SMAP radar.

The SMAP L2SMAP product also includes ancillary and quality related data fields. A description of these fields is provided in the SMAP L2SMAP Product Specification Document available through NSIDC. Some examples of this information are shown in Figs. 11 and 12. A typical SMAP swath, shown in Fig. 11, is associated with a soil moisture retrieval quality flag for every EASE2 grid cell at 9 km and 3 km. A flag value of 0 represents good quality and any value greater than 0 represents substandard quality due to surface flags or due to a quality flag associated with the disaggregated T_{B_p} or due to the quality of the input data ($T_{B_p}(C)$ and σ_{pp} and σ_{pq}). Fig. 12 illustrates the surface flags associated with each and every soil moisture retrieval. The surface flags are stored in the bits (0 means clear and 1 mean present) of a 2 bytes integer. The example shows the flag value of 0 or 1 for any given grid cell that represents the existence of the particular surface condition (*e.g.*, static waterbodies, coastal region, urban flag, and terrain flag). However, the surface flag also contains information about the transient nadir flag, as shown in Fig. 12.

4. L2SMAP product validation

4.1. Core validation sites

The SMAP L2SMAP validation was based primarily on comparison of retrievals with *in situ* soil moisture measurements (Colliander et al., 2017; Chan et al., 2016). Other validation methodologies, such as evaluation against model outputs and comparison with other satellites soil moisture retrievals were not used because of a limited number of retrievals (~2.5 months) available for the L2SMAP product. The *in situ* measurements for the top ~5 cm from soil moisture networks with an acceptable sensor density within a 9 km EASE2 grid were the primary validation locations for the L2SMAP product. The SMAP project collaborated with various partners from around the world to identify such locations and established CVS (Colliander et al., 2017). These CVS have been verified as providing a spatial average of soil moisture at 9 km and 3 km spatial resolutions. However, the spatial averages of soil moisture from CVS are not without issues because of inherent upscaling errors. Table 1 lists the CVS as well as potential sites known as candidate sites that do not meet the requirements or level of maturity to become CVS

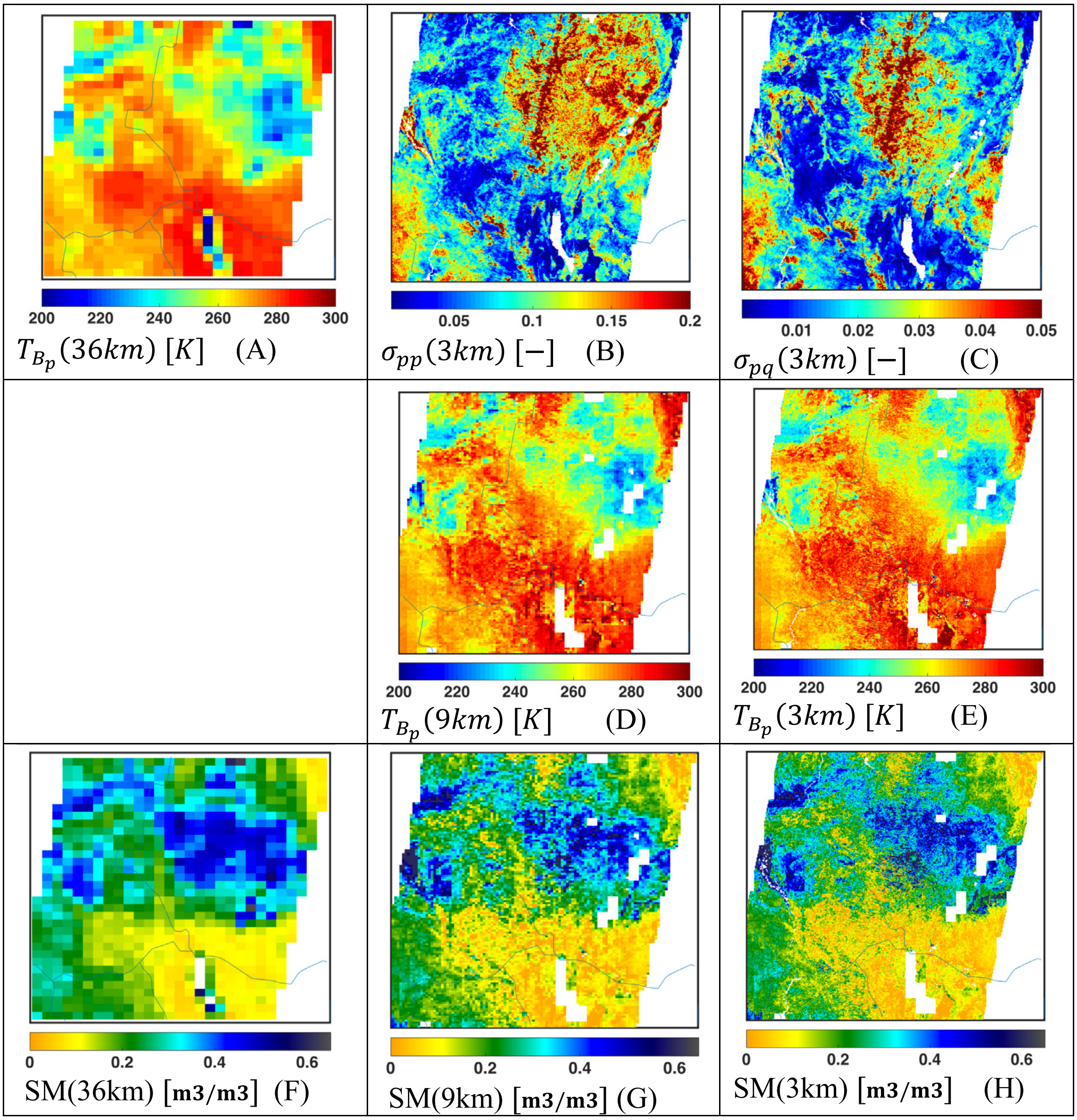

Fig. 10. Illustration of the enhancement of spatial details of soil moisture provided by the L2SMAP algorithm on July 1st, 2015 (Central and Western Ethiopia, and Western part of Kenya). The inputs and outputs from the SMAP active-passive algorithm are: A) input coarse resolution brightness temperature $T_{B_v}(C)$ at 36 km; B) input high resolution (9 km or 3 km) co-pol backscatter $\sigma_{pp}(M_j)$; C) input high resolution (9 km or3 km) co-pol backscatter $\sigma_{pq}(M_j)$; D) output disaggregated brightness temperature $T_{B_v}(M)$ at 9 km; E) output disaggregated brightness temperature $T_{B_v}(M)$ at 3 km; F) soil moisture SM (36 km) retrieval from coarse resolution brightness temperature $T_{B_v}(C)$ at 36 km, SMAP radiometer-only product; G) soil moisture SM (9 km) retrievals from the disaggregated $T_{B_v}(M)$ at 9 km resolution; and H) soil moisture SM (3 km) retrievals from the disaggregated $T_{B_v}(M)$ at 3 km resolution.

during the period of this investigation. Beside the CVS, sparse networks (Chen et al., 2017) were also used as a supporting tool to validate the L2SMAP product. More details about the L2SMAP validation are provided in the SMAP Active-Passive Product Assessment report, available through NSIDC (https://nsidc.org/sites/nsidc.org/files/technical-references/SMAPSPBetaReleaseAssessmentReport_11-01-2017_final.pdf).

Figs. 13, 14, and 15 show comparisons and statistics of L2SMAP 9 km grid cells for three CVS: Little Washita, TxSON, and Valencia, respectively. Similar comparisons and statistics were performed for the L2SMAP 9 km grid cells against the suitable CVS sites. Overall, 10 CVS (two Yanco and two TxSON sites were averaged) were used as primary validation for the L2SMAP product. Some of the CVS (*e.g.*, South Fork) over the Midwest region of CONUS were not included because the SMAP radar measurements were suspected of having artifacts due to unresolved radio frequency interference (RFI). These RFI signatures introduced errors in the backscatter observations leading erroneous disaggregated brightness temperature. The time series plot in Fig. 13 for the Little Washita shows a good match between soil moisture trends, with some bias in soil moisture retrievals, especially when the vegetation is high during the summer months. The performance of the L2SMAP product over most of the CVS with non-crop landcovers is reasonable as illustrated in Fig. 14 for TxSON and Fig. 15 for Valencia. However, the performance of the L2SMAP over CVS with crop cover is inferior, possibly because of being out of sync with the vegetation attribute information. The retrieval process uses vegetation-water-content (VWC) derived from the NDVI climatology (developed from 10 years of MODIS data), which might lead to a mismatch with the actual status of VWC. Therefore, it is likely that in Fig. 13, Little Washita CVS the lack of a consistent bias and has higher errors may be

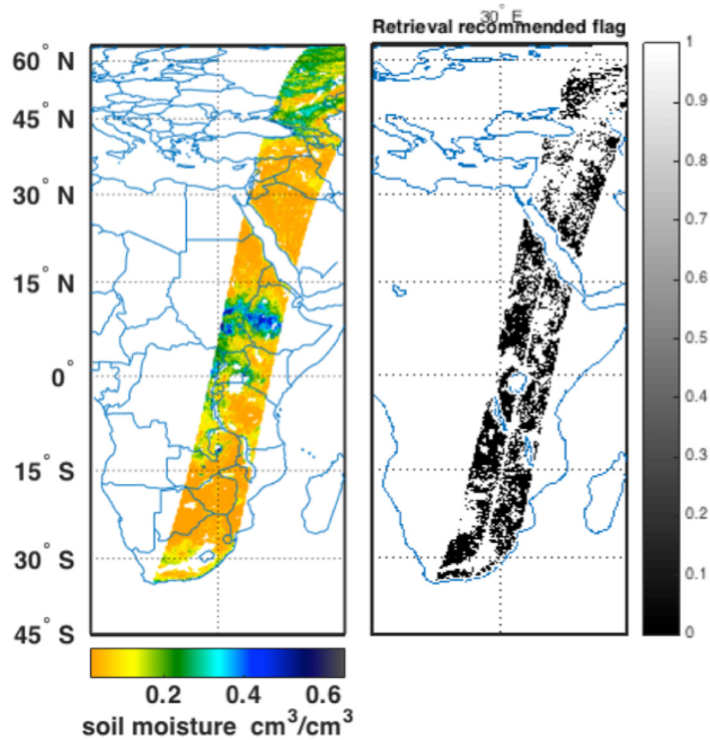

Fig. 11. A typical L2SMAP swath (June 6th, 2015) with associated retrieval quality flag. Pixels that do not have any flags are plotted in black.

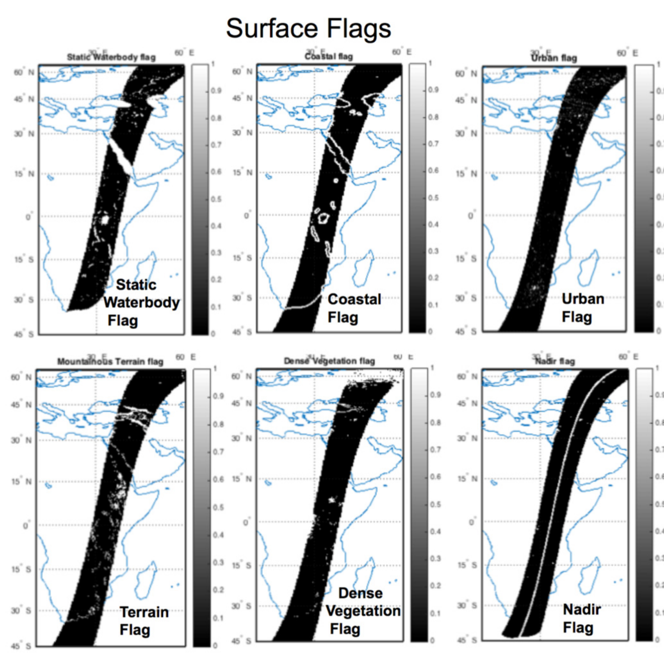

Fig. 12. Surface flags of L2SMAP swath (June 6th, 2015) in the L2SMAP product. Pixels that do not have any specific flags are plotted in black.

caused by the mismatch.

Table 2 shows the comparison statistics (correlation 'R', root-mean-square-error "RMSE", 'Bias', and unbiased root-mean-squared-error "ubRMSE") between the CVS upscaled soil moisture averages and the L2SMAP soil moisture retrievals for the T_{B_v} 9 km options. The term RMSE in the analysis is interchangeably used for root-mean-square-difference (RMSD). However, RMSD is more appropriate because the upscaled CVS value is not the truth. Most of the R-values in Table 2 are relatively high and exhibit a good match of the trend. The overall ubRMSE of 0.039 m^3/m^3 for Option-1 T_{B_v} at 9 km meets the SMAP

Table 1
SMAP Cal/Val partner sites providing validation data.

Site name	Site PI	Area	Climate regime	IGBP land cover	Status
Walnut Gulch[a]	C. Holifield Collins	USA (Arizona)	Arid	Shrub open	**Used in validation**
Reynolds Creek[b]	M. Seyfried	USA (Idaho)	Arid	Grasslands	Short data length due to snow cover
Fort Cobb	P. Starks	USA (Oklahoma)	Temperate	Grasslands	Lesser number of *in situ* sensors at 9 km
Little Washita[a]	P. Starks	USA (Oklahoma)	Temperate	Grasslands	**Used in validation**
South Fork[c]	M. Cosh	USA (Iowa)	Cold	Croplands	SMAP SAR σ has artifacts
Little River[a]	D. Bosch	USA (Georgia)	Temperate	Cropland/natural mosaic	**Used in validation**
TxSON[a]	T. Caldwell	USA (Texas)	Temperate	Grasslands	**Used in validation**
Millbrook	M. Temimi	USA (New York)	Cold	Deciduous broadleaf	Lesser number of *in situ* sensors at 9 km
Tonzi Ranch[b]	M. Moghaddam	USA (California)	Temperate	Savannas	**Used in validation**
Kenaston[a]	A. Berg	Canada	Cold	Croplands	**Used in validation**
Carman[c]	H. McNairn	Canada	Cold	Croplands	SMAP SAR σ has artifacts
Monte Buey[a]	M. Thibeault	Argentina	Arid	Croplands	**Used in validation**
Bell Ville	M. Thibeault	Argentina	Arid	Croplands	Lesser number of *in situ* sensors at 9 km
REMEDHUS	J. Martinez	Spain	Temperate	Croplands	Lesser number of *in situ* sensors at 9 km
Valencia[a]	E. Lopez-Beaza	Spain	Arid	Shrub (open)	**Used in validation**
Twente	Z. Su	Holland	Cold	Cropland/natural mosaic	Lesser number of *in situ* sensors at 9 km
Kuwait	H. Jassar	Kuwait	Temperate	Barren/sparse	Lesser number of *in situ* sensors at 9 km
Niger	T. Pellarin	Niger	Arid	Grasslands	Lesser number of *in situ* sensors at 9 km
Benin	T. Pellarin	Benin	Arid	Savannas	Lesser number of *in situ* sensors at 9 km
Naqu	Z. Su	Tibet	Polar	Grasslands	Lesser number of *in situ* sensors at 9 km
Maqu	Z. Su	Tibet	Cold	Grasslands	Lesser number of *in situ* sensors at 9 km
Ngari	Z. Su	Tibet	Arid	Barren/sparse	Lesser number of *in situ* sensors at 9 km
MAHASRI	JAXA	Mongolia	Cold	Grasslands	Lesser number of *in situ* sensors at 9 km
Yanco[a]	J. Walker	Australia	Arid	Croplands	**Used in validation**
Kyeamba	J. Walker	Australia	Temperate	Croplands	Lesser number of *in situ* sensors at 9 km

[a] CVS used in assessment.
[b] Reynolds Creek, the length of record was too short due to snow cover.
[c] Not used because artifacts were found in the SAR data.

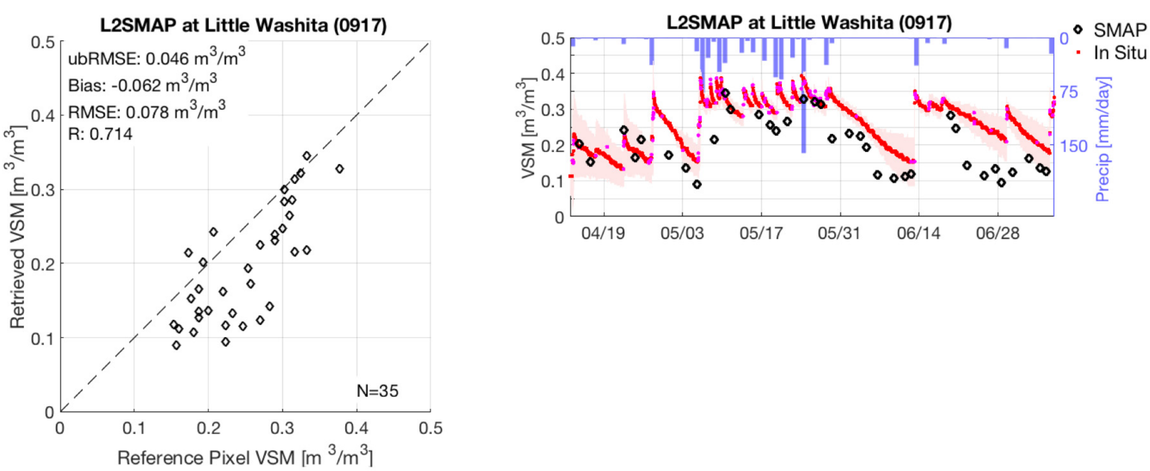

Fig. 13. L2SMAP Assessment for Little Washita, Oklahoma, USA.

mission goal of 0.04 m^3/m^3. Similar statistics were also developed for all the options of T_{B_H} at 9 km, and T_{B_V} and T_{B_H} at 3 km (not shown). From the statistics of all the soil moisture retrievals from options at 9 km and at 3 km for T_{B_V} and T_{B_H} (total 8 options), the Option-1 at 9 km for T_{B_V} based soil moisture retrievals has very comparable ubRMSE and the highest R-value, therefore, it is considered as the primary soil moisture product and the associated disaggregation approach as the L2SMAP baseline algorithm. Nonetheless, the soil moisture retrievals performed for disaggregated T_{B_V} at 3 km that were compared to CVS measurements had an ubRMSE of ~0.053 m^3/m^3, which suggests that the 3 km L2SMAP is a promising soil moisture product.

We also assessed the contribution of the SAR radar observations in the SMAP active-passive algorithm. There are two ways to approach this evaluation: 1) by comparing the disaggregated brightness temperature (T_{B_V} *at* 9 *km*) with the high-resolution brightness temperature observed through an airborne platform, and evaluating against the coarse resolution brightness temperature (T_{B_V} *at* 36 *km*) observed by the SMAP radiometer; and 2) comparing the soil moisture retrievals from L2SMAP and minimum performance (MP) against a CVS. The MP is simply obtained by setting $\boldsymbol{\beta}(C) = 0$ in Eq. (1) (SMAP active-passive algorithm) of the manuscript. In other words, MP is simply applying the coarse resolution T_{B_V} (*at* 36 *km*) value to all 9 km cells.

The first approach was presented in Leroux et al. (2016) and Leroux et al. (2017) that the SMAP active-passive algorithm outperforms the MP in brightness temperature space. Table 3 shows the performance of L2SMAP against the MP. The statistics show that the SMAP active-

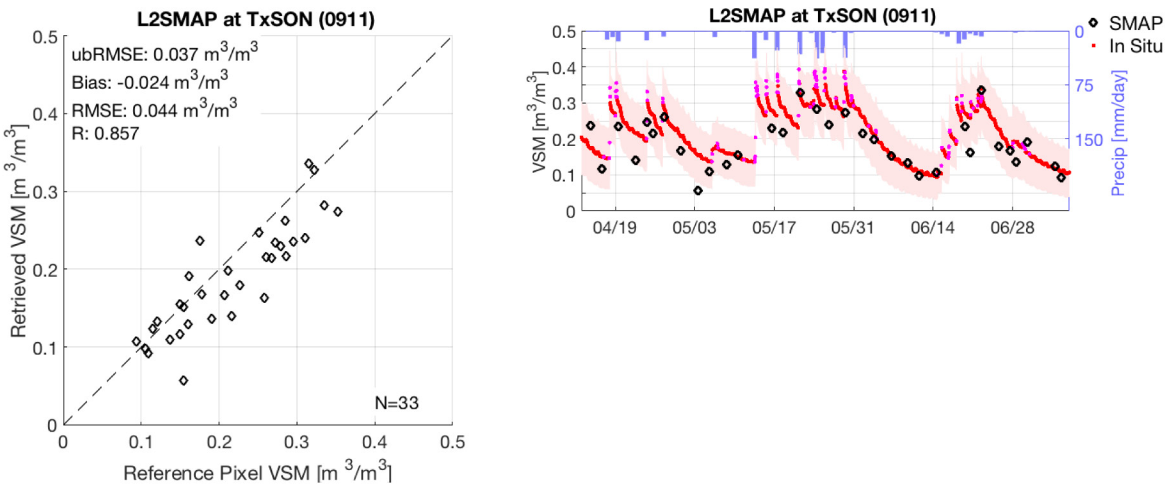

Fig. 14. L2SMAP Assessment for TxSON, Texas, USA.

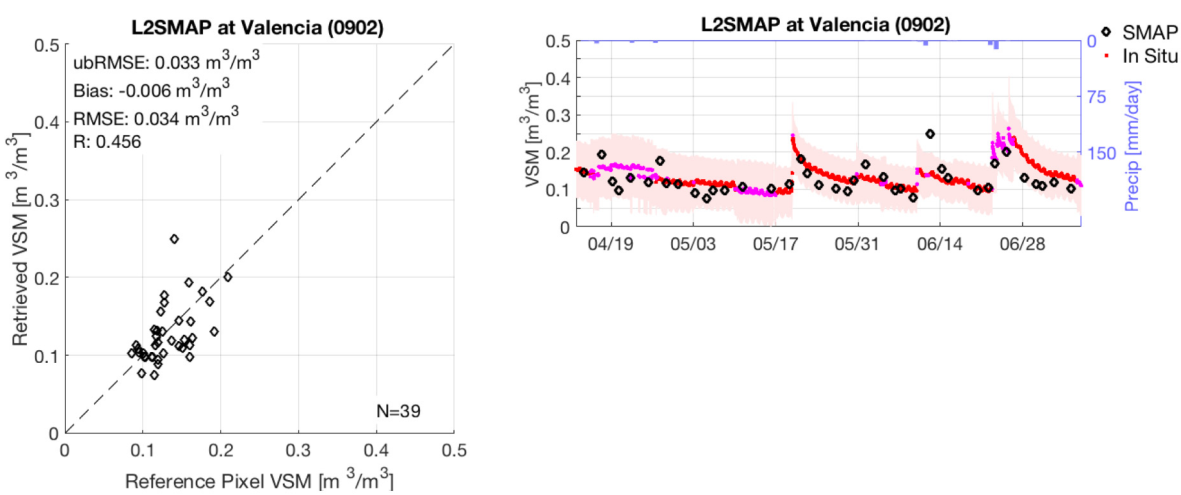

Fig. 15. L2SMAP Assessment for Valencia, Spain.

passive algorithm clearly outperforms (better ubRMSE, Bias, and RMSE) the MP in most of the CVS sites except the highly vegetated regions.

4.2. Sparse soil moisture networks

The intensive CVS validation performed for the SMAP L2SMAP can be complemented by sparse networks as well as by new/emerging types of soil moisture networks. The important difference in interpreting these data is that they involve one *in situ* point in a grid cell. Thus, whatever reservations there might be on the upscaling for the CVS are of greater concern with sparse networks. However, sparse networks do offer many sites in different environments.

The established soil moisture networks utilized for the SMAP L2SMAP comparison were the NOAA Climate Reference Network (CRN), the USDA NRCS Soil Climate Analysis Network (SCAN), the Oklahoma Mesonet, the MAHASRI network (in Mongolia), the SMOSMania network (in southwest Europe), the Pampas network (in Argentina), and soil moisture estimates derived from the surface reflectance at Global Position Stations (in the Western US). From these sparse soil moisture networks, 311 sites were found to be suitable for direct comparison with the SMAP L2SMAP overlapping grid cells. The 311 sites were selected based on *in situ* measurement data quality and continuity of the observations during the 2.5 months period (April 14th, 2015 to July 7th, 2015). The defining feature of these networks were the low measurement density that usually resulted in one point per L2SMAP 9 km grid cell that leads to large upscaling errors in the ability of a single site location to describe mean soil moisture within a 3 or 9-km grid cell. The SMAP Project evaluated methodologies for upscaling measurements from these networks to SMAP defined grid resolutions.

Table 2
SMAP L2SMAP validated release assessment for disaggregated T_{B_v} at 9 km.

Site name	ubRMSE (m^3/m^3)			Bias (m^3/m^3)			RMSE (m^3/m^3)			R		
	Opt-1	Opt-2	Opt-3	Opt-1	Opt-2	Opt-3	Opt-1	Opt-2	Opt-3	Opt-1	Opt-2	Opt-3
Walnut Gulch	0.016	0.015	0.026	−0.019	−0.019	−0.011	0.024	0.025	0.029	0.190	0.187	0.59
TxSON (2 core sites)	0.042	0.042	0.039	−0.005	−0.007	−0.005	0.047	0.047	0.043	0.860	0.862	0.87
Tonzi Ranch	0.022	0.022	0.022	−0.037	−0.037	−0.038	0.043	0.043	0.044	0.837	0.837	0.836
Little Washita	0.046	0.045	0.045	−0.062	−0.071	−0.071	0.078	0.084	0.084	0.714	0.705	0.719
Little River	0.026	0.026	0.031	0.066	0.066	0.094	0.071	0.071	0.099	0.764	0.764	0.718
Kenaston	0.042	0.042	0.043	0.002	0.002	0.002	0.042	0.042	0.043	0.489	0.489	0.481
Monte Buey	0.067	0.067	0.064	0.021	0.021	0.019	0.071	0.071	0.067	0.904	0.909	0.895
Valencia	0.033	0.033	0.033	−0.006	−0.006	−0.009	0.034	0.034	0.034	0.456	0.456	0.456
Yanco (2 core sites)	0.057	0.055	0.061	0.037	0.041	0.037	0.073	0.071	0.074	0.698	0.740	0.710
SMAP Average	0.039	0.039	0.041	−0.001	−0.001	0.002	0.053	0.054	0.057	0.66	0.66	0.69
Averages are based on the values reported for each CVS												

Table 3
SMAP L2SMAP baseline (BL that is Opt-1) compared against the minimum performance (MP) at 9 km.

Site name	ubRMSE (m^3/m^3)		Bias (m^3/m^3)		RMSE (m^3/m^3)		R	
	BL	MP	BL	MP	BL	MP	BL	MP
Walnut Gulch	0.016	0.036	−0.019	−0.016	0.024	0.035	0.190	0.86
TxSON	0.042	0.039	−0.005	−0.033	0.047	0.055	0.860	0.84
Tonzi Ranch	0.022	0.032	−0.037	−0.068	0.043	0.076	0.837	0.75
Little Washita	0.046	0.045	−0.062	−0.053	0.078	0.072	0.714	0.825
Little River	0.026	0.032	0.066	0.06	0.071	0.069	0.764	0.67
Kenaston	0.042	0.063	0.002	−0.033	0.042	0.07	0.489	0.611
Monte Buey	0.067	0.058	0.021	−0.001	0.071	0.059	0.904	0.929
Valencia	0.033	0.038	−0.006	−0.039	0.034	0.055	0.456	0.5
Yanco (2 core sites)	0.057	0.062	0.037	0.036	0.073	0.081	0.698	0.85
SMAP average	0.039	0.045	−0.001	−0.0163	0.053	0.064	0.66	0.76
Averages are based on the values reported for each CVS								

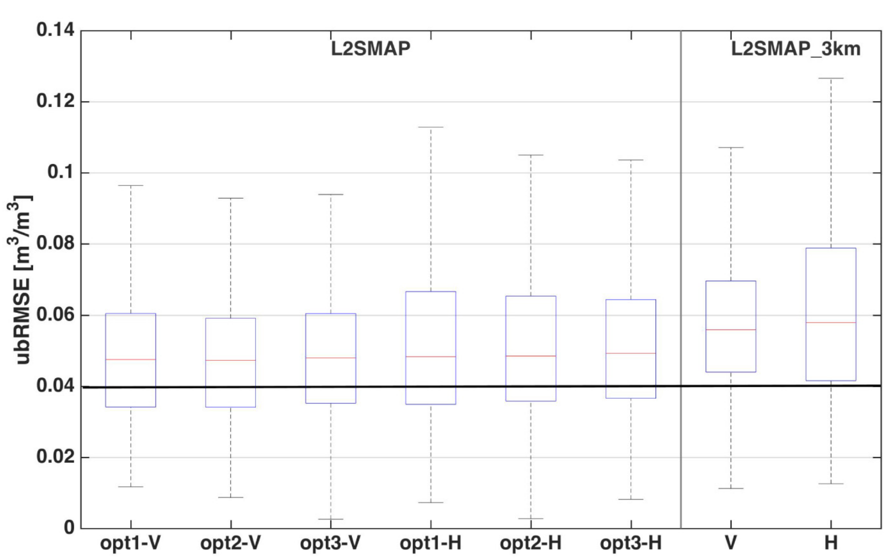

A)

Fig. 16. Results of comparison between L2SMAP with the sparse network sites (311 *in situ* sites): A) unbiased RMSE; and B) correlation for L2SMAP soil moisture retrievals for all algorithm options.

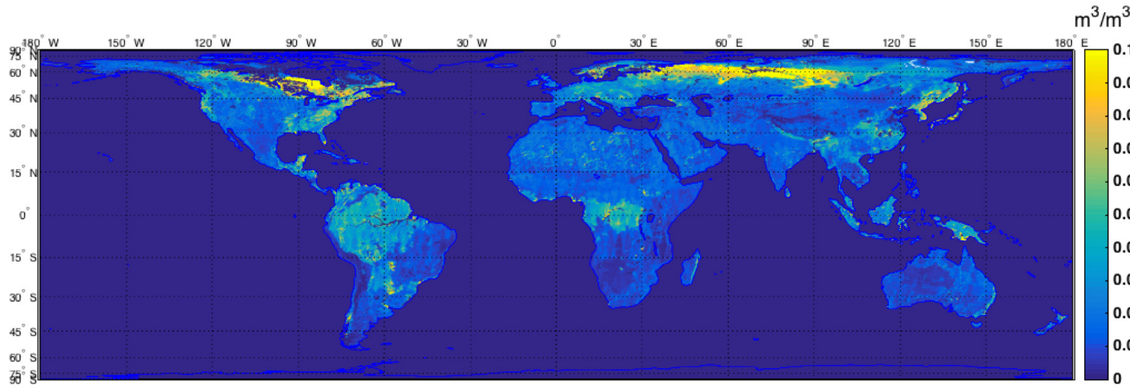

Fig. 17. Comparison of L2SMAP and L2SMP soil moisture (modulus of absolute difference) without using retrieval quality flags.

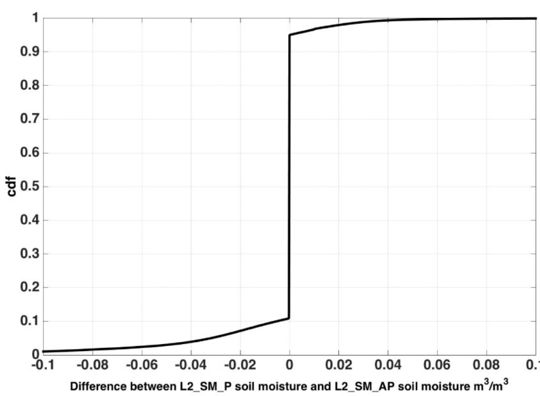

Fig. 18. CDF of the absolute difference between the L2SMAP and L2SMP soil moisture computed from the whole month of June 2015 that included ~800 half orbits.

Due to the very short data record for the L2SMAP product, these approaches could not be applied here. However, despite this source of bias, sparse networks can adequately describe relative errors (existing *e.g.* between various algorithm versions). In addition, sparse networks do offer many sites in different environments.

The L2SMAP product retrievals available for 311 global sparse network sites from many different landcovers were compared with *in situ* observations. Fig. 16 cross-compares the metrics of all options of the L2SMAP (9 km and 3 km) products. Despite the potential errors associated with spatial representativeness, the ubRMSE and bias values obtained from these sparse networks are similar to those obtained from the CVS. These results (Fig. 16) provide further confidence in the previous conclusions based on the CVS. In addition, the SMAP L2SMAP TBV Option-1 has one of the best overall ubRMSE and correlation as compared to all other options algorithms implemented at 9 km and 3 km.

4.3. Consistency with the 36 km SMAP radiometer-only product

Intercomparison of the SMAP L2SMAP soil moisture with the L2SMP soil moisture is useful in assessment of the L2SMAP because both use the same radiative-transfer-model and brightness temperature data in their respective algorithms. The soil moisture product from the descending pass (6 AM) L2SMP was matched with the L2SMAP descending pass product. For comparison, the L2SMAP soil moisture at 9 km is averaged to 36 km EASE2 grid using a drop-in-a-bucket (averaging all the 9 km grid cells within the overlapping 36 km grid cell) technique. Retrieval quality flags provided in the respective product files are applied to both L2SMAP and L2SMP to allow comparison of high-quality soil moisture retrievals. The data available for the entire L2SMAP period was used in this intercomparison. Fig. 17 shows that there is good agreement between the L2SMAP (averaged to 36 km) and the 36 km L2SMP soil moisture estimates for the 30 day period. The differences in the L2SMAP and L2SMP are within the acceptable limit because soil moisture upscaling by averaging is not purely linear. Noticeable differences at 36 km are visible only over regions with high vegetation, for example over forests (Amazon, Congo basin), and sandy bare soil with rock outcrops (as visible in the Sahara Desert). Fig. 18 presents the results of Fig. 17 using cumulative density function (CDF) for both products. The CDF shows almost no difference in soil moisture retrievals between the L2SMAP (9 km averaged to 36 km) and the L2SMP grid cells for nearly 85% of the global landmass. The differences, of -0.06 to $0.04\ m^3/m^3$, is mostly found in the highly vegetated regions and is expected because of the nonlinear nature of Tau-Omega parameters when applied at 9 km and 36 km spatial scales.

5. Discussion

The SMAP observatory is a first of its kind mission that delivered coincident and collocated measurements using an L-band radar and an L-band radiometer. This provided a unique opportunity to obtain the status of geophysical information such as soil moisture at much higher spatial resolutions than previously possible using satellite remote sensing. The SMAP active-passive algorithm was able to achieve the mission goal by producing high-resolution soil moisture (L2SMAP) at 9 km and 3 km. A validated release of the SMAP L2SMAP data to NSDIC also meets the SMAP mission requirements. However, some further potential for improvement in the SMAP L2SMAP data quality may be possible by reducing the errors in soil moisture retrievals. These include further optimizing the Tau-Omega model parameters for various landcovers at resolutions of 9 km and 3 km. Currently, the SMAP L2SMAP retrievals use the same Tau-Omega parameters as the L2SMP retrievals at 36 km. Another important step to improving the L2SMAP data quality is the inclusion of retrieved vegetation-optical-depth (VOD) or Tau. The Tau values used for L2SMAP retrievals were derived from a 10-year climatology of NDVI based VWC (Tau = b*VWC, b is a parameter based on landcover, typically close to 0.1). The drawback of using VWC climatology for Tau is prominently visible over CVS with cropland landcover. Using a retrieved Tau or alternatively, the real VWC (based on real NDVI) instead of climatological value may help reduce the high ubRMSE observed for cropland regions. Another possibility for improving the L2SMAP product is through the inclusion of the most recent SMAP radar backscatter data for σ_{pp} and σ_{pq} and the L1CS0HiRes products that will also have the unresolved RFI issue fixed that are present over the Midwest region of North America. This will enable inclusion of

CVS such as South Fork and Carman where problems with RFI were identified.

6. Conclusion

The active-passive algorithm developed during the SMAP prelaunch period using field campaigns airborne data was successfully implemented on the SMAP radiometer and radar data available for ~2.5 months period. Six alternative active-passive algorithm options at 9 km and two active-passive algorithm options at 3 km were implemented, and retrievals were performed on the disaggregated/downscaled brightness temperatures. The retrieved soil moisture estimates were then validated using CVS comparisons supplemented by Sparse Networks with metrics and time series plots. These analyses indicated that the Option-1 (T_{B_v}) has better and comparable unbiased root-mean-square-errors (ubRMSE), bias, and correlation R than the rest of algorithms. Option-1 (T_{B_v}) also had one of the best performances in the sparse network analysis. Based on the results, it is recommended that the Option-1 (T_{B_v}) be adopted as the baseline algorithm for the SMAP active-passive algorithm. In the CVS analysis, the overall ubRMSE of the Option-1 (T_{B_v}) is 0.039 m^3/m^3, which is close to the SMAP mission requirement. SMAP L2SMAP retrievals were also compared globally with the SMAP L2SMP retrievals. The agreement between the L2SMAP retrievals and the L2SMP retrievals is good. Some of the observed differences are expected in areas where more surface heterogeneity exists or over highly vegetated regions. Intercomparisons using the other SMAP option algorithms indicated similar performance. Further improvement in the SMAP L2SMAP product is also possible through optimizing the parameters and also by improving the input ancillary information used in soil moisture retrievals. The SMAP Project plans to release an updated and improved SMAP L2SMAP product in future. However, the current SMAP L2SMAP product at 9 km and 3 km in NSDIC is good for use in geophysical applications and research.

Acknowledgements

The research was carried out at the Jet Propulsion Laboratory (JPL), CaliforniaInstitute of Technology, under a contract with the National Aeronautics andSpace Administration (NASA). We acknowledge the sustained support from the SMAP Project at JPL, and the Earth Science section of the NASA HQ. We acknowledge the support of Dr. Steven Chan and Dr. Seungbum Kim from JPL for their constructive comments and help in developing some of the modules for the SMAP active-passive Science Software. We also acknowledge contributions of many staff and personnel who helped in acquiring calibration and validation data that are used for this work.

References

Chan, S., Bindlish, R., O'Neill, P., Njoku, E.G., Jackson, T.J., Colliander, A., Chen, F., Bürgin, M., Dunbar, S., Piepmeier, J., Yueh, S., Entekhabi, D., Cosh, M., Caldwell, T., Walker, J., Wu, X., Berg, A., Rowlandson, T., Pacheco, A., McNairn, H., Thibeault, M., Martínez- Fernández, J., González-Zamora, Á., Seyfried, M., Bosch, D., Starks, P., Goodrich, D., Prueger, J., Palecki, M., Small, E., Calvet, J.-C., Crow, W., Kerr, Y., 2016. Assessment of the SMAP level 2 passive soil moisture product. IEEE Trans. Geosci. Remote Sens. 54 (8), 4994–5007.

Chauhan, N.S., Miller, S., Ardanuy, P., 2003. Space borne soil moisture estimation at high resolution: a microwave-optical/IR synergistic approach. Int. J. Remote Sens. 24 (22), 4599–4622.

Chen, F., Crow, W.T., Colliander, A., Cosh, M., Jackson, T.J., Bindlish, R., Reichle, R., Chan, S.K., Bosch, D.D., Starks, P.S., Goodrich, D.C., Seyfried, M.S., 2017. Application of triple collocation in ground-based validation of soil moisture active/passive (SMAP) level 2 data products. IEEE J. Sel. Top. Appl. Earth Obs. Remote Sensing 10, 489–502.

Colliander, A., Jackson, T.J., Bindlish, R., Chan, S., Das, N.N., Kim, S.B., Cosh, M.H., Dunbar, R.S., Dang, L., Pashaian, L., Asanuma, J., Aida, K., Berg, A., Rowlandson, T., Bosch, D., Caldwell, T., Caylor, K., Goodrich, D., al Jassar, H., Lopez-Baeza, E., Martinez-Fernandez, J., Gonzalez-Zamora, A., Livingston, S., McNairn, H., Pacheco, A., Moghaddam, M., Montzka, C., Notarnicola, C., Niedrist, G., Pellarin, T., Prueger, J., Pulliainen, J., Rautiainen, K., Ramo, J., Seyfried, M., Starks, P., Su, Z., Zeng, Y., van der Velde, R., Thibeault, M., Dorigo, W., Vreugdenhil, M., Walker, J.P., Wu, X., Monerris, A., O'Neill, P.E., Entekhabi, D., Njoku, E.G., Yueh, S., 2017. Validation of SMAP surface soil moisture products with core validation sites. Remote Sens. Environ. 191, 215–231.

Das, N.N., Entekhabi, D., Njoku, E.G., 2012. An algorithm for merging SMAP radiometer and radar data for high resolution soil moisture retrieval. IEEE Trans. Geosci. Remote Sens. 9, 1504–1512.

Das, N.N., Entekhabi, D., Njoku, E.G., Johnston, J., Shi, J.C., Colliander, A., 2014. Tests of the SMAP combined radar and radiometer brightness temperature disaggregation algorithm using airborne field campaign observations. IEEE Trans. Geosci. Remote Sens. 52, 2018–2028.

Entekhabi, D., Njoku, E.G., O'Neill, P., Kellogg, K., Crow, W., Edelstein, W., Entin, J., Goodman, S., Jackson, T., Johnson, J., Kimball, J., Peipmeier, J., Koster, R., McDonald, K., Moghaddam, M., Moran, S., Reichle, R., Shi, J., Spencer, M., Thurman, S., 2010. The soil moisture active and passive (SMAP) mission. Proc. IEEE 98, 704–716.

Jagdhuber, T., Entekhabi, D., Hajnsek, I., Konings, A., McColl, K., Alemohammad, H., Das, N.N., Montzka, C., 2015. Active-passive modelling and retrieval for SMAP soil moisture inversion algorithm. IEEE Trans. Geosci. Remote Sens. Symposium (IGARSS)pp. 1300–1303 (Milan).

Kim, G., Barros, A.P., 2002. Space-time characterization of soil moisture from passive microwave remotely sensed imagery and ancillary data. Remote Sens. Environ. 81, 393–403.

Kim, G., Barros, A.P., 2003. Downscaling of remotely sensed soil moisture with a modified fractal interpolation method using contraction mapping and ancillary data. Remote Sens. Environ. 83, 400–413.

Kim, Y., van Zyl, J., 2009. A time series approach to estimate soil moisture using polarimetric radar data. IEEE Trans. Geosci. Remote Sens. 47, 2519–2527.

Leroux, D., Das, N.N., Entekhabi, D., Colliander, A., Njoku, E.G., Jackson, T.J., Yueh, S., 2016. Active-passive disaggregation of brightness temperatures during the SMAPVEX12 campaign. IEEE Trans. Geosci. Remote Sens. 54, 6859–6867.

Leroux, D., Das, N.N., Entekhabi, D., Colliander, A., Njoku, E.G., Jackson, T.J., Yueh, S., 2017. Active–passive soil moisture retrievals during the SMAP validation experiment 2012. Geosci. Remote Sens. Lett. 13, 475–479.

Merlin, O., Walker, J.P., Chehbouni, A., Kerr, Y., 2008. Towards deterministic downscaling of SMAO soil moisture using MODIS derived soil evaporative efficiency. Remote Sens. Environ. 112, 3935–3946.

Molero, B., Merlin, O., Malbéteau, Y., Al Bitar, A., Cabot, F., Stefan, V., Jackson, T.J., 2016. SMOS disaggregated soil moisture product at 1 km resolution: processor overview and first validation results. Remote Sens. Environ. 180, 361–376.

Narayan, U., Lakshmi, V., Jackson, T.J., 2006. High resolution estimation of soil moisture using L-band radiometer and radar observations made during the SMEX02 experiments. IEEE Trans. Geosci. Remote Sens. 44, 1545–1554.

Piles, M., Entekhabi, D., Camps, A., 2009. A change detection algorithm for retrieving high resolution soil moisture from SMAP radar and radiometer observations. IEEE Trans. Geosci. Remote Sens. 47, 4125–4131.

Reichle, R.H., Entekhabi, D., McLaughlin, D.B., 2001. Downscaling of radio brightness measurements for soil moisture estimation: a four dimensional variational data assimilation approach. Water Resour. Res. 37 (9), 2353–2364.

Zhan, X., Houser, P.R., Walker, J.P., Crow, W.T., 2006. A method or retrieving high-resolution surface soil moisture from hydros L-band radiometer and radar observations. IEEE Trans. Geosci. Remote Sens. 44, 1534–1544.